JCTC Journal of Chemical Theory and Computation
Article
pubs.acs.org/JCTC

Analytic Derivatives of Quartic-Scaling Doubly Hybrid XYGJ-OS Functional: Theory, Implementation, and Benchmark Comparison with M06-2X and MP2 Geometries for Nonbonded Complexes

Hyunjun Ji,[†] Yihan Shao,[‡] William A. Goddard,[†,§] and Yousung Jung*[,†]

[†]Graduate School of EEWS, KAIST, Daejeon 305-701, Republic of Korea
[‡]Q-Chem Inc., Pittsburgh, Pennsylvania 15213, United States
[§]Department of Chemistry, California Institute of Technology, Pasadena, California 91106, United States

ABSTRACT: Analytic first derivative expression of opposite-spin (OS) ansatz-adapted quartic scaling doubly hybrid XYGJ-OS functional is derived and implemented into Q-Chem. The resulting algorithm scales quartically with system size as in OS-MP2 gradient, by utilizing the combination of Laplace transformation and density fitting technique. The performance of XYGJ-OS geometry optimization is assessed by comparing the bond lengths and the intermolecular properties in reference coupled cluster methods. For the selected nonbonded complexes in the S22 and S66 data sets used in the present benchmark test, it is shown that XYGJ-OS geometries are more accurate than M06-2X and RI-MP2, the two quantum chemical methods widely used to obtain accurate geometries for practical systems, and comparable to CCSD(T) geometries.

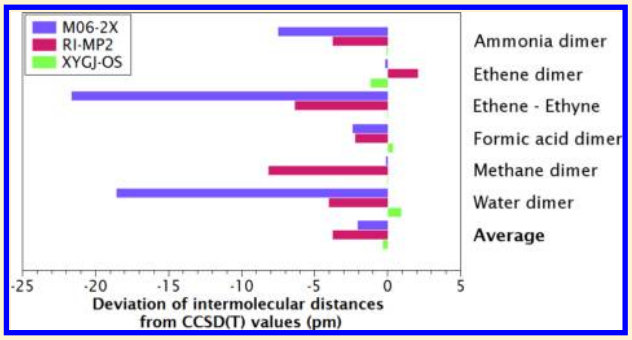

1. INTRODUCTION

Obtaining higher accuracy with lower computational cost has been the goal of quantum chemistry community. Among them, Kohn−Sham density functional theory (KS-DFT)[1] is presently the most widely used approach, due to its mild scaling in computational time and reasonable energy values. However, the exchange−correlation functionals, whose exact form is yet unknown, must be approximated. Many approximated density functionals have well-known inherent deficiencies, for instance, lack of description of van der Waals interaction, self-interaction errors, and abnormal behavior for fractional charge/spin cases.[2] Until now, several treatments have been suggested for the problem of missing long-range correlation in semilocal density functionals, such as addition of semiempirical interatomic pairwise dispersion correction,[3,4] calculation of dispersion energies based on multipole moments,[5,6] or van der Waals density functional correction with nonlocal kernel.[7] However, it still remains as an open question whether these semiempirical long-range corrections are capable of fully recovering correlations that the semilocal functionals fail to capture. While none of the practical density functionals has satisfactorily solved the problems including aforementioned notorious lack of nonlocality or reached the area of so-called "chemical accuracy", the systematic method for improvement of density functionals is still unknown. Thus, we expect there is still a long way to go before DFT becomes a "gold standard" method for quantum chemistry.

In the last two decades, second-order perturbative expansion schemes on top of hybrid density functionals, including Görling−Levy perturbation theory[8] and perturbation theory starting from density scaled hybrid functionals,[9] have been developed and tested. Such approaches yield MP2-like postcorrection term for density functionals and results in schemes generally called doubly hybrid density functionals (DHDF's).[10−19] They not only compensate missing nonlocal correlation term but also are expected to give a better estimate of true energy because the energy is perturbatively corrected over the existing density functional scheme. In addition to their accuracy in ground-state calculations, DHDF's are also known as the most accurate schemes among density functionals for low-lying excited-state calculations.[13,20,21] However, most of them suffer from formal scaling of $O(N^5)$, originating from MP2-like correction, which is sometimes called PT2 correction. The practical computational cost may be reduced by using smaller basis sets for the PT2 postcorrection[10,22] with reparametrization of the functional, however, the fundamental fifth-order scaling is unaltered in such approaches with only the prefactor reduced. Recently suggested XYGJ-OS functional[23] shows a reduced quartic scaling by approximating PT2 energy term with OS-MP2 ansatz,[24] utilizing auxiliary basis set expansion[25] and Laplacian quadrature technique,[26] like earlier OS-MP2 ansatz-based DHDF's.[15,18] Practically, calculation of OS-PT2 energy, hence total XYGJ-OS energy can be implemented with cubic scaling with numerical cutoff technique for low-dimensional systems.[27] The accuracy of the OS ansatz in XYGJ-OS, while being computationally less demanding, was shown to be comparable to that of its conventional PT2 counterpart XYG3.[17] Though it shares some

Received: January 21, 2013
Published: March 4, 2013

   dx.doi.org/10.1021/ct400050d | J. Chem. Theory Comput. 2013, 9, 1971−1976

problems with most of commonly used density functionals, like self-interaction error or inability to describe large static correlations, XYGJ-OS provided the similar level of accuracy to that of XYG3 for G3 benchmark set[23] and noncovalent benchmark sets,[28] while slightly deterioriating in terms of consistency for noncovalent systems.

In this study, we present the derivation of analytic first-order energy derivatives of XYGJ-OS functional, which also can be calculated with quartic scaling. An outline of relevant theories will be presented in Section 2. In Section 3, to test the accuracy of XYGJ-OS optimized geometries, both intramolecular and intermolecular properties are calculated and compared with other methods.

2. THEORY

In this section, working expressions for analytic gradient of quartic-scaling OS-PT2 corrected doubly hybrid functionals are derived and discussed. Though the results are presented in only a spin-restricted manner for the sake of brevity, their extension to a spin-unrestricted case is not of much complication. The fine details of derivation will not be provided here, since XYGJ-OS energy gradient is essentially an assembly of doubly hybrid functional gradient[29] and OS-MP2 gradient,[30] whose details are already presented elsewhere.

Throughout this paper, indices $i, j, \ldots$ refer to occupied orbitals, $a, b, \ldots$ to virtual orbitals, and $p, q, \ldots$ to general orbitals. $K, L, \ldots$ are auxiliary basis functions for density fitting ,and $\mu, \nu, \kappa, \ldots$ indicate atom-centered basis functions, while σ and σ' correspond to spin variables.

2.1. Review of XYGJ-OS Energy Evaluation. The energy expression for XYGJ-OS doubly hybrid functional is written as

$$E_{xc}^{\text{XYGJ-OS}} = 0.7731E_x^{\text{HF}} + 0.2269E_x^{S} + 0.2309E_c^{\text{VWN}} + 0.2754E_c^{\text{LYP}} + 0.4364E_c^{\text{OS-PT2}} \tag{1}$$

where relevant Kohn−Sham orbitals and density are obtained from a B3LYP calculation. Here, OS-PT2 is PT2 analogue of OS-MP2, which means only opposite spin components of PT2 correlation energy are calculated and scaled by a constant. The OS-PT2 energy is written as

$$E_c^{\text{OS-PT2}} = -\sum_{ia}^{\alpha}\sum_{jb}^{\beta}\frac{(ia|jb)^2}{\Delta_{ij}^{ab}} = -\sum_{ia}^{\alpha}\sum_{jb}^{\beta}\int_0^{\infty}(ia|jb)^2\ \exp(-\Delta_{ij}^{ab}t)\mathrm{d}t \tag{2}$$

where $(ia|jb) = \int\phi_i^*(\mathbf{x}_1)\phi_j^*(\mathbf{x}_2)r_{12}^{-1}\phi_a(\mathbf{x}_1)\phi_b(\mathbf{x}_2)\mathrm{d}\mathbf{x}_1\mathrm{d}\mathbf{x}_2$, $\Delta_{ij}^{ab} = \varepsilon_a + \varepsilon_b - \varepsilon_i - \varepsilon_j$, and the exponential term comes from the identity $x^{-1} = \int_0^{\infty}\exp(-xt)\mathrm{d}t$. The integral over t can be approximated as a summation over t along Laplacian quadrature:

$$E_c^{\text{OS-PT2}} = -\sum_{ia}^{\alpha}\sum_{jb}^{\beta}\sum_{q}w_q(ia|jb)^2\ \exp(-\Delta_{ij}^{ab}t_q) \tag{3}$$

where q represents each quadrature point and w_q is weight of the point. Density fitting scheme allows us to approximate two-electron integrals as

$$(ia|jb) = \sum_K B_{ia}^K B_{jb}^K \tag{4}$$

where $B_{ia}^K = \sum_L (ia|L)(L|K)^{-1/2}$. Then with the quadrature-dependent quantity:

$$X_{KL}^{q,\sigma} = \sum_{ia}^{\sigma}\exp\{(\varepsilon_i - \varepsilon_a)t_q\}B_{ia}^K B_{ia}^L \tag{5}$$

OS-PT2 energy expression can be written again as

$$E_c^{\text{OS-PT2}} = -\sum_{ia}^{\alpha}\sum_{jb}^{\beta}\sum_{KL}\sum_{q}w_q\ \exp(-\Delta_{ij}^{ab}t_q)B_{ia}^K B_{jb}^K B_{ia}^L B_{jb}^L = -\sum_{KL}\sum_{q}w_q X_{KL}^{q,\alpha}X_{KL}^{q,\beta} \tag{6}$$

Here, the formation of X consumes computational time proportional to only fourth power of system size,[24] therefore scaling of calculation of the total OS-PT2 energy is quartic, in contrast to quintic scaling of conventional or density fitted MP2.

2.2. Derivation of XYGJ-OS Analytic Gradients. The XYGJ-OS energy can be separated into three parts:

$$E^{\text{XYGJ-OS}} = E^{\text{B3LYP}} + \Delta E_{xc} + c_{\text{OS-PT2}}E_c^{\text{OS-PT2}} \tag{7}$$

where $\Delta E_{xc} \equiv E^{\text{XYGJ-OS}} - E^{\text{B3LYP}} - c_{\text{OS-PT2}}E_c^{\text{OS-PT2}}$ consists of only hybrid density functional part of postcorrection. The XYGJ-OS gradient is, of course, the sum of gradients of these three components.

2.2.1. Hybrid Functional Part. The first-order derivative of hybrid functionals, B3LYP in this case, is already well-known:[31]

$$E_{\text{SCF}}^x = E_{\text{SCF}}^H H^x + E_{\text{SCF}}^{\Pi}\Pi^x + E_{\text{SCF}}^S S^x = P\cdot H^x + \Gamma\cdot\Pi^x + W_{\text{SCF}}\cdot S^x + E_{xc}^{(x)} \tag{8}$$

where H is the one-electron Hamiltonian, P is the one-body density matrix, $\Gamma = 1/2P \otimes P$ is the two body density matrix, S is the overlap matrix, and $W = -PFP$ is the energy-weighted density matrix.

2.2.2. ΔE_{xc} Part. Since ΔE_{xc} does not depend on core integrals, its derivative with respect to an external variable is simply

$$\Delta E_{xc}^x = \Delta E_{xc}^{\Pi}\Pi^x + \Delta E_{xc}^S S^x + \Delta E_{xc}^{\Theta}\Theta^x \tag{9}$$

where Θ stands for orbital rotation. More specifically, mixing between occupied and virtual orbitals will affect ΔE_{xc}. Here, variationality of SCF energy guarantees its Lagrangian is zero, i.e. $E_{\text{SCF}}^{\Theta} = 0$. Then,

$$(E_{\text{SCF}}^{\Theta})^x = E_{\text{SCF}}^{\Theta H}H^x + E_{\text{SCF}}^{\Theta\Pi}\Pi^x + E_{\text{SCF}}^{\Theta S}S^x + E_{\text{SCF}}^{\Theta\Theta}\Theta^x = 0 \tag{10}$$

which leads to

$$\Theta^x = -(E_{\text{SCF}}^{\Theta\Theta})^{-1}[E_{\text{SCF}}^{\Theta H}H^x + E_{\text{SCF}}^{\Theta\Pi}\Pi^x + E_{\text{SCF}}^{\Theta S}S^x] \tag{11}$$

By defining the z-vector[32] as

$$E_{\text{SCF}}^{\Theta\Theta}z = L = \Delta E_{xc}^{\Theta} = \Delta F_{xc}\cdot P^{\Theta} \tag{12}$$

where $\Delta F_{xc} = \Delta E_{xc}^P$, we can rewrite the derivative of ΔE_{xc} as

$$\Delta E_{xc}^x = z\cdot P^{\Theta}\cdot H^x + \left[\Delta E_{xc}^{\Pi} + \left(\frac{1}{2}P\otimes P\right)^{\Theta}\cdot z\right]\cdot\Pi^x + (\Delta E_{xc}^S + W_{\text{SCF}}^{\Theta}\cdot z)\cdot S^x \tag{13}$$

By defining P_z as $P_z = z\cdot P^{\Theta} = C_v z C_o^{\dagger} + c.c.$, each component of gradient expression can be written in a concise fashion:

$$\Delta E_{xc}^{\Pi} + \left(\frac{1}{2}P\otimes P\right)^{\Theta}\cdot z = \frac{1}{2}a_x^{\Delta_{xc}}P\otimes P + P\otimes P_z \tag{14}$$

$$\Delta E_{xc}^S + W_{\text{SCF}}\cdot z = -\frac{1}{2}(CC^{\dagger}\Delta F'P + P\Delta F'CC^{\dagger})\cdot S^x \tag{15}$$

where

Table 1. Experimental and Calculated Bond Lengths (Å) in the MGBL19 Database[a]

molecule	bond	expt[b]	HF	PBE	B3LYP	M06-2X	RI-MP2	SOS-MP2	XYGJ-OS
H_2	H−H	0.741	0.734	0.751	0.743	0.742	0.736	0.737	0.743
CH_4	C−H	1.086	1.082	1.096	1.088	1.086	1.072	1.084	1.087
NH_3	N−H	1.012	0.998	1.021	1.013	1.012	1.008	1.010	1.010
H_2O	O−H	0.957	0.940	0.969	0.961	0.958	0.956	0.958	0.957
HF	H−F	0.917	0.897	0.930	0.922	0.918	0.916	0.916	0.917
CO	C−O	1.128	1.102	1.131	1.125	1.120	1.132	1.129	1.130
N_2	N−N	1.098	1.066	1.103	1.091	1.086	1.108	1.103	1.101
F_2	F−F	1.412	1.327	1.411	1.395	1.363	1.395	1.412	1.416
C_2H_2	C−C	1.203	1.179	1.207	1.196	1.193	1.206	1.204	1.205
	C−H	1.063	1.054	1.071	1.062	1.063	1.059	1.060	1.062
HCN	C−H	1.065	1.057	1.075	1.066	1.067	1.062	1.062	1.066
	C−N	1.153	1.123	1.158	1.146	1.142	1.160	1.157	1.157
H_2CO	C−H	1.102	1.093	1.117	1.106	1.103	1.097	1.097	1.101
	C−O	1.203	1.176	1.209	1.199	1.195	1.206	1.205	1.205
CO_2	C−O	1.160	1.134	1.171	1.159	1.154	1.164	1.161	1.162
N_2O	N−N	1.128	1.081	1.137	1.121	1.111	1.148	1.137	1.136
	N−O	1.184	1.168	1.189	1.183	1.179	1.175	1.178	1.185
OH	O−H	0.970	0.950	0.983	0.974	0.970	0.964	0.965	0.968
Cl_2	Cl−Cl	1.988	1.978	2.009	2.013	1.986	1.982	2.000	1.998
MUE			−0.023	0.009	−0.000	−0.006	−0.001	0.000	0.002
MAE			0.027	0.009	0.005	0.007	0.006	0.004	0.003

[a]Wavefunction calculations and density functional calculations were performed with cc-pVQZ and G3Large basis set, respectively. [b]Ref 35.

$$\Delta F' = \Delta F_{xc} + P_z\cdot\Pi + P_z\cdot F_{xc}^{P} \tag{16}$$

Therefore, the final working equation is

$$\Delta E_{xc}^{x} = P_z\cdot H^x + \frac{1}{2}a_x^{\Delta E_{xc}} P\cdot\Pi^x\cdot P + P\cdot\Pi^x\cdot P_z - \frac{1}{2}(CC^{\dagger}\Delta F' P + P\Delta F' CC^{\dagger})\cdot S^x \tag{17}$$

2.2.3. OS-PT2 Part. The gradient of OS-PT2 energy can be constructed from OS-MP2 gradient[30] and PT2 gradient.[29] Direct differentiation of OS-PT2 expression[24] leads to

$$\begin{aligned}
-\frac{1}{2}E_{\text{OS-PT2}}^{x} &= \sum_{ia}^{\alpha}\sum_{KL}\sum_{q} w_q e^{(\varepsilon_i-\varepsilon_a)t_q}[(\varepsilon_i^{x}-\varepsilon_a^{x})t_q \\
&\quad - (M|K)^{-1/2}(M|K)^{x}]B_{ia}^{K}B_{ia}^{L}X_{KL}^{q,\beta} \\
&\quad + 2\sum_{ia}^{\alpha}\sum_{KL}\sum_{q} w_q e^{(\varepsilon_i-\varepsilon_a)t_q}(ia|M)^{x}(M|K)^{-1/2}B_{ia}^{L}X_{KL}^{q,\beta} \\
&= \sum_{ia}^{\alpha}\sum_{KL}\sum_{q} w_q e^{(\varepsilon_i-\varepsilon_a)t_q}[(\varepsilon_i^{x}-\varepsilon_a^{x})t_q \\
&\quad - (M|K)^{-1/2}(M|K)^{x}]B_{ia}^{K}B_{ia}^{L}X_{KL}^{q,\beta} \\
&\quad + 2\sum_{ia}^{\alpha}\sum_{KL}\sum_{q} w_q e^{(\varepsilon_i-\varepsilon_a)t_q}(ia|M)^{(x)}(M|K)^{-1/2}B_{ia}^{L}X_{KL}^{q,\beta} \\
&\quad + 2\sum_{ia}^{\alpha}\sum_{KL}\sum_{q} w_q e^{(\varepsilon_i-\varepsilon_a)t_q}(\Theta_{pi}^{x}B_{pa}^{K}+\Theta_{pa}^{x}B_{ip}^{K})B_{ia}^{L}X_{KL}^{q,\beta}
\end{aligned} \tag{18}$$

While the other parts are relatively easy to calculate as they involve less theoretical and computational complications, the trickiest part is Θ^x, as in our earlier treatment of the hybrid density functional part of the XYGJ-OS energy correction. The orbital response can be calculated by CP-SCF equation:

$$\sum_{ai} A'_{aibj}\Theta_{ai}^{x} \equiv \sum_{ai}[\delta_{ab}\delta_{ij}(\varepsilon_i-\varepsilon_a)+A_{aibj}]\Theta_{ai}^{x} = B_{bj}^{x} \tag{19}$$

where

$$\begin{aligned}
A_{pqrs} &\equiv 4[pr|qs] - a_x([pq|rs]+[pr|sq]) + F_{ai}^{P_{bj}} \\
B_{pq}^{x} &\equiv F_{pq}^{(x)} - S_{pq}^{(x)}\varepsilon_q - \frac{1}{2}\sum_{ij} S_{ij}^{x}A_{pqij}
\end{aligned} \tag{20}$$

Practically, instead of the CP-SCF equation, the z-vector equation[32] is constructed and solved, since $3N$ CP-SCF equations, each of which corresponds to one degree of freedom of nuclear, can be reduced into a single equation: CP-SCF equation $A'\Theta^x = B^x$ is reduced to the z-vector equation $A^{T'}z = L$, where $L \equiv E^{\Theta}$ is Lagrangian. Then the orbital responses, if needed, can be calculated from z with less computational cost. The Lagrangian for OS-PT2 is

$$L_{\text{OS-PT2}} = L_{\text{OS-MP2}} + \sum_{pq} A_{aipq}D'_{pq} \tag{21}$$

where D' is "unrelaxed" PT2 difference density matrix. Here, Lagrangian corresponding to Hartree−Fock component of OS-MP2 is replaced by corresponding DFT part, since OS-PT2 energy depends on Kohn−Sham orbitals, instead of Hartree−Fock orbitals. Having solved z-vector equation, we obtain "relaxed" PT2 difference density matrix $D = D' + z$.

Making use of these, after some algebraic manipulations, final OS-PT2 gradient expression follows, which is similar to RI-MP2 gradient:

$$E_{\text{OS-PT2}}^{x} = D\cdot H^x + \frac{1}{2}P\cdot\Pi^{(x)}\cdot P + W_{\text{OS-PT2}}\cdot S^{(x)} + \sum_{\mu\nu}\sum_{K}\Gamma_{\mu\nu}^{K}(\mu\nu|K)^{x} + \sum_{KL}\gamma_{KL}(K|L)^{x} + D\cdot(F_{xc}^{P})^{x} \tag{22}$$

dx.doi.org/10.1021/ct400050d | J. Chem. Theory Comput. 2013, 9, 1971−1976

where $\Gamma^{K}_{\mu\nu}$ and γ_{KL} are RI-specific 2-PDM's. More details of OS-MP2 gradient are described elsewhere.[30]

3. RESULTS

3.1. Implementation. We have implemented the quartic scaling XYGJ-OS analytic gradient calculation into the latest version of quantum chemical software package, Q-Chem.[33] In principle, XYGJ-OS analytic gradient can be implemented straightforwardly into any package including gradient codes of hybrid DFT and auxiliary basis OS-MP2. ΔE_{xc} codes can be written making use of existing hybrid DFT gradient and z-vector equation solver codes, and a proper modification is required in z-vector equation of OS-MP2 part, which involves some changes in A_{pqrs}, as described above. Details of auxiliary basis OS-MP2 gradients and doubly hybrid functional gradients are described elsewhere.[29,30]

3.2. Applications. *3.2.1. Bond Lengths.* To investigate the performance of XYGJ-OS functional for small molecules, MGBL19 benchmark[34] set has been chosen. MGBL19 is a database containing 15 small main-group molecules and 19 experimental bond lengths, which also has been used for parametrization of M06-L functional.[34]

Performances of selected wave function-based theories and density functional methods including XYGJ-OS are summarized in Table 1. The results show that XYGJ-OS functional gives the smallest MAE for the prediction of small main-group compounds, outperforming B3LYP, M06-2X, RI-MP2, and SOS-MP2. On the other hand, the magnitude of MUE of XYGJ-OS was larger than those of B3LYP, RI-MP2, and SOS-MP2. This indicates that XYGJ-OS tends to overestimate bond lengths by ~0.2 pm, however, also shows concentrated distribution of errors.

3.2.2. Noncovalent Interactions. Unlike intramolecular properties, intermolecular properties, such as the distance between weakly bound molecules, are particularly troublesome to predict with currently used methods. B3LYP, for example, is known to yield often qualitatively wrong results for dispersion dominant systems. Therefore, such systems are usually calculated with correlated ab initio methods, such as MP2 or CCSD(T). However, MP2 is generally known as an overbinding scheme, and CCSD(T) optimization with sufficiently large basis is often too costly to be applied to any practical systems containing more than 10−20 heavy atoms. Need for counterpoise correction in geometry optimization is another hindrance for those methods to be attractive. Thus, highly accurate optimization methods being able to manage nonbonding interactions should be of great interest.

To test quality of geometries involving noncovalent interactions, 20 complexes with low molecular weights are selected from S22[36] and S66[37] data sets. These 20 complexes are seven hydrogen-bonded complexes, seven dispersion-dominant systems, and six other complex classified as "others" in original papers.

Since plain hybrid density functionals are unable to describe noncovalent interactions, functionals parametrized with long-range interactions in the training set should be chosen to compare with XYGJ-OS. Among many such functionals, perhaps the most widely used one is M06-2X, considering its extensive use in the chemistry community, hence we chose it. It is proven to yield low (<0.3 kcal/mol) mean absolute error (MAE) for the S66 set even without additional empirical dispersion corrections.[38] A wave function theory counterpart that is perhaps most widely used for both energy calculation and geometry optimization is MP2 (or RI-MP2), and so we also chose it for geometry comparsion. We note that the majority of reference geometries in the S22 and S66 database have been optimized with RI-MP2.

The selected 20 complexes were optimized with M06-2X, RI-MP2, and XYGJ-OS. Then, for the latter total 60 complex geometries, CCSD(T)-F12(b) calculations were performed with cc-pVnZ (n = 2−4) level. In other words, we explored where in the CCSD(T)-F12(b) potential energy surfaces the M06-2X, RI-MP2, and XYGJ-OS geometries locate themselves. Hartree−Fock energies were exponentially extrapolated, and correlation energies were also extrapolated where possible. Parameters for correlation energy extrapolation were taken from the study of Hill et al.[39] for VnZ-F12 basis.

For M06-2X hybrid meta-GGA functional, aug-cc-pVTZ basis set is used in this study, and RI-MP2 optimizations are performed with cc-pVTZ level. The basis set for XYGJ-OS calculations are G3Large, as suggested in functional optimization, especially considering that doubly hybrid functionals are known to be heavily basis set dependent. Euler−Maclaurin radial grid with 120 points and Lebedev angular grid with 194 points are applied for DFT calculations, since M06-2X functional is somewhat grid dependent. Tight optimization criteria (energy change 1×10^{-8} au, maximum gradient component 1×10^{-5} au, maximum atomic displacement 5×10^{-5} au) were used for high-quality geometries. Counterpoise correction was applied only to RI-MP2 optimizations but not for M06-2X and XYGJ-OS. M06-2X and XYGJ-OS calculations were performed with Q-Chem,[33] and MP2 and CCSD(T)-F12(b) calculations were performed with MOLPRO.[40]

Table 2. Relative CCSD(T)-F12(b) Energies (kcal/mol) at Geometries Optimized with M06-2X, RI-MP2, and XYGJ-OS[a]

		nature	M06-2X	RI-MP2	XYGJ-OS	
ammonia	-ammonia	H	0	0.02	0.01	TQ-F12 CBS
formic acid	-formic acid	H	0.17	0.12	0	TQ-F12 CBS
$MeNH_2$	-water	H	0.03	0.01	0	DT-F12 CBS
MeOH	-water	H	0.05	0.04	0	TQ-F12 CBS
water	-$MeNH_2$	H	0.04	0.32	0	DT-F12 CBS
water	-MeOH	H	0.07	0.04	0	TQ-F12 CBS
water	-water	H	0.03	0.02	0	TQ-F12 CBS
benzene	-benzene	D	0.36	0	0.37	DZ-F12
benzene	-pyridine	D	0.30	0	0.11	DZ-F12
ethene	-ethene	D	0.29	0.16	0	TQ-F12 CBS
ethene	-pentane	D	0.24	0	0.01	DZ-F12
methane	-methane	D	0.02	0.08	0	TQ-F12 CBS
pyridine	-ethene	D	0.30	0	0.01	DZ-F12
benzene	-ethene	O	0.31	0	0.06	DZ-F12
benzene	-ethyne	O	0.28	0	0.01	DZ-F12
ethene	-ethyne	O	0.24	0.12	0	TQ-F12 CBS
ethyne	-AcOH	O	0.20	0.12	0	DZ-F12
ethyne	-water	O	0.15	0.02	0	TQ-F12 CBS
peptide	-ethene	O	0.21	0.18	0	DZ-F12
average			0.18	0.06	0.02	

[a]The lowest energy among the latter three geometries is set to 0. The last column denotes the level of correlation energy calculation. TQ-F12 CBS denotes the cc-pV(TQ)Z-F12 extrapolation to the CBS limit using CCSD(T)-F12 method. DZ-F12 denotes CCSD(T)-F12/cc-pVDZ-F12 without extrapolation due to large system sizes.

In Table 2, relative energies of optimized geometries for each complex are listed. For example, for ammonia dimer, M06-2X geometry has the lowest CCSD(T)-F12(b) energy, and the CCSD(T)-F12(b) energy of XYGJ-OS geometry is 0.01 kcal/mol higher than that. Thus, M06-2X geometry was of the best quality, and RI-MP2 geometry was the worst among the three methods for the ammonia dimer. The result shows that XYGJ-OS geometries have the lowest energy overall, i.e., XYGJ-OS geometries are the best in quality. For most cases, even if XYGJ-OS geometry was not the most stable, its energy did not deviate from the lowest one more than 0.1 kcal/mol, with the exception being the benzene dimer. RI-MP2 geometries with counterpoise correction recorded average relative energy of 0.06 kcal/mol, while M06-2X geometries are generally higher in energy despite their widespread use for geometry optimization. However, it is also noteworthy that for the most of cases where XYGJ-OS performed poorly, the single point CCSD(T)-F12(b) energies were calculated with cc-pVDZ-F12 basis only due to system sizes, thus no extrapolation was performed. It is possible that further extrapolation might change the result for such cases.

Although there are not many nonbonded systems that have been optimized with CCSD(T) in literature, there are several small molecular complexes that were optimized with CCSD(T) in the S22 and S66 database. Thus we next compared the XYGJ-OS geometries directly with the CCSD(T) geometries for these small complexes. Table 3 shows energies of optimized geometries relative to CCSD(T) geometries. On average, the energies of XYGJ-OS geometries deviate only 0.02 kcal/mol from those CCSD(T) geometries. Interestingly for the formic acid dimer, XYGJ-OS geometry even yielded a lower energy structure than CCSD(T)/cc-pVTZ geometry. At least based on these limited test cases, it appears that XYGJ-OS geometries are very comparable to CCSD(T)/cc-pVnZ (n = 3, 4) geometries.

The comparison of intermolecular distances of three sets of geometries with CCSD(T) geometries is presented in Table 4. In terms of distances between the centers of mass of monomers, XYGJ-OS shows the least errors in terms of both MUE and MAE, deviating only some tenth of picometers. Again, this geometry result shows that XYGJ-OS optimization gives very accurate geometries comparable to CCSD(T) optimizations.

3.3. Benchmark Timing. For hydrogen terminated diamond-like systems, B3LYP, XYGJ-OS, and B2PLYP gradient timings are benchmarked. To avoid system dependencies and complications, gradient timing is defined as a subtraction of SCF timing from total timing. Since B2PLYP gradient is currently unavailable for Q-Chem, we estimated the B2PLYP gradient timing as a sum of B3LYP and RI-MP2 gradient timings. The 6-31G* basis set was used for calculation to emphasize the scaling behavior depending on system size, though the recommended basis set for XYGJ-OS is G3Large.

In Figure 1, B3LYP, XYGJ-OS, and B2PLYP gradient timings for diamond-like systems are plotted. As shown in the figure, since the timing difference between XYGJ-OS and B2PLYP originates from that of RI-MP2 and SOS-MP2, XYGJ-OS is always faster than B2PLYP. Though formal quartic scaling of XYGJ-OS and quintic

Table 3. CCSD(T)-F12(b) Energies at Geometries Optimized with M06-2X, RI-MP2, and XYGJ-OS for Relatively Small-Sized Systems[a]

		nature	M06-2X	RI-MP2	XYGJ-OS	
ammonia	-ammonia	H	0.04	0.06	0.05	cc-pVQZ
formic acid	-formic acid	H	0.10	0.05	−0.07	cc-pVTZ
water	-water	H	0.03	0.02	0.00	cc-pVQZ
ethene	-ethene	D	0.32	0.19	0.03	cc-pVQZ
methane	-methane	D	0.02	0.09	0.00	cc-pVTZ
ethene	-ethyne	O	0.25	0.13	0.02	cc-pVQZ
average			0.18	0.06	0.02	

[a]The CCSD(T)-F12(b)/CBS energies at CCSD(T) optmized geometries are used as reference. The last column denotes the basis set used in the CCSD(T) optimization. Negative values for the formic acid dimer in XYGJ-OS means that, in the CCSD(T)-F12(b)/CBS potential energy surfaces, the XYGJ-OS geometry is lower in energy than the CCSD(T)/cc-pVTZ geometry.

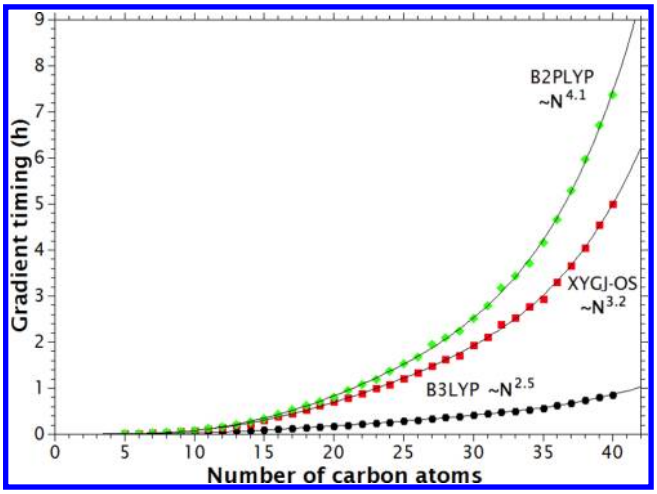

Figure 1. Single-step gradient timings of B3LYP, XYGJ-OS, and B2PLYP for hydrogen terminated diamond-like systems, plotted with respect to number of carbon atoms.

Table 4. Intermolecular Distances (Å) between the Center of Mass of Monomers for Geometries Optimized with Various Methods[a]

		nature	CCSD(T)[36]	M06-2X	RI-MP2	XYGJ-OS
ammonia	-ammonia	H	3.209	3.188	3.171	3.206
formic acid	-formic acid	H	3.718	3.533	3.678	3.727
water	-water	H	4.422	4.421	4.340	4.421
ethene	-ethene	D	2.993	2.969	2.971	2.995
methane	-methane	D	3.718	3.502	3.654	3.718
ethene	-ethyne	O	2.909	2.908	2.929	2.898
MUE				−0.075	−0.037	−0.000
MAE				0.075	0.044	0.004

[a]Errors (MUE and MAE) are calculated by setting the CCSD(T) values as reference.

dx.doi.org/10.1021/ct400050d | J. Chem. Theory Comput. 2013, 9, 1971−1976

scaling of RI-MP2 is not shown explicitly due to the use of relatively small molecular systems for timing comparison, it is clearly seen that the scaling of XYGJ-OS is milder than that of conventional DHDF calculations containing full PT2 correction. Incidentally, we note that the use of numerical derivatives for XYGJ-OS would scale as N^5 instead of N^4 as in the present analytic derivative technique.

4. CONCLUSIONS

The analytic gradients expression for quartic-scaling XYGJ-OS doubly hybrid functional is presented. By its construction, the derivative scale quartically with system size, as in OS-MP2 gradient. Hence, the adaptation of OS-MP2 scheme in DHDF's leads to significant computational speedups not only for single point energy calculations but also for gradients calculations. Moreover, since XYGJ-OS has been parametrized to partly overcome basis set incompleteness for G3Large basis set, additional computational complication, such as counterpoise correction, is not required.

Among methods which scale not steeper than quartic scaling tested in this paper, XYGJ-OS gives the least MAE for bond lengths for main group compounds. It is also shown that for nonbonded complexes XYGJ-OS geometries are more accurate than M06−2X and RI-MP2, quantum chemistry methods that are widely used for obtaining accurate geometries, and quite comparable to CCSD(T)/cc-pVTZ or CCSD(T)/cc-pVQZ geometries. We expect XYGJ-OS gradients offer a reasonably economical method for calculating highly accurate geometries and force field fitting.

AUTHOR INFORMATION

Corresponding Author

*E-mail: ysjn@kaist.ac.kr

Notes

The authors declare no competing financial interest.

ACKNOWLEDGMENTS

We are pleased to acknowledge the support of Basic Science Research (2010-0023018) and WCU (R-31-2008-000-10055-0) programs funded by the Ministry of Education, Science, and Technology of Korea. Y.S. acknowledges financial support from NIH through SBIR grant no. GM096678 and Prof. Martin Head-Gordon for helpful discussions. We also thank Dr. Igor Ying Zhang and Prof. Xin Xu for helpful discussions. We acknowledge the generous supercomputing time from KISTI.

REFERENCES

(1) Kohn, W.; Sham, L. J. *Phys. Rev.* **1965**, *140*, A1133.
(2) Cohen, A. J.; Mori-Sánchez, P.; Yang, W. *Science* **2008**, *321*, 792.
(3) Grimme, S.; Antony, J.; Ehrlich, S.; Krieg, H. *J. Chem. Phys.* **2010**, *132*, 154104.
(4) Kim, H.; Choi, J.-M.; Goddard, W. A. *J. Phys. Chem. Lett.* **2012**, *3*, 360.
(5) Johnson, E. R.; Becke, A. D. *J. Chem. Phys.* **2006**, *124*, 174104.
(6) Sato, T.; Nakai, H. *J. Chem. Phys.* **2009**, *131*, 224104.
(7) Vydrov, O. A.; Van Voorhis, T. V. *J. Chem. Phys.* **2010**, *133*, 244103.
(8) Görling, A.; Levy, M. *Phys. Rev. A* **1994**, *50*, 196.
(9) Sharkas, K.; Toulouse, J.; Savin, A. *J. Chem. Phys.* **2011**, *134*, 064113.
(10) Zhao, Y.; Lynch, B. J.; Truhlar, D. G. *J. Phys. Chem. A* **2004**, *108*, 4786−4791.
(11) Zhao, Y.; Lynch, B. J.; Truhlar, D. G. *Phys. Chem. Chem. Phys.* **2005**, *7*, 43−52.
(12) Grimme, S. *J. Chem. Phys.* **2006**, *124*, 034108.
(13) Grimme, S.; Neese, F. *J. Chem. Phys.* **2007**, *127*, 154116.
(14) Karton, A.; Tarnopolsky, A.; Lamère, J.-F.; Schatz, G. C.; Martin, J. M. L. *J. Phys. Chem. A* **2008**, *112*, 12868.
(15) Benighaus, T.; DiStasio, R. A.; Lochan, R. C.; Chai, J.-D.; Head-Gordon, M. *J. Phys. Chem. A* **2008**, *112*, 2702.
(16) Chai, J.-D.; Head-Gordon, M. *J. Chem. Phys.* **2009**, *131*, 174105.
(17) Zhang, Y.; Xu, X.; Goddard, W. A. *Proc. Natl. Acad. Sci. U.S.A.* **2009**, *106*, 4963−4968.
(18) Goerigk, L.; Grimme, S. *J. Chem. Theory Comput.* **2011**, *7*, 291.
(19) Zhang, I. Y.; Su, N. Q.; Bremond, E. A. G.; Adamo, C.; Xu, X. *J. Chem. Phys.* **2012**, *136*, 174103.
(20) Goerigk, L.; Moellmann, J.; Grimme, S. *Phys. Chem. Chem. Phys.* **2009**, *11*, 4611.
(21) Goerigk, L.; Grimme, S. *J. Chem. Theory Comput.* **2011**, *7*, 3272.
(22) Karton, A.; Martin, J. M. L. *J. Chem. Phys.* **2011**, *135*, 144119.
(23) Zhang, I. Y.; Xu, X.; Jung, Y.; Goddard, W. A. *Proc. Natl. Acad. Sci. U.S.A.* **2011**, *108*, 19896.
(24) Jung, Y.; Lochan, R. C.; Dutoi, A. D.; Head-Gordon, M. *J. Chem. Phys.* **2004**, *121*, 9793.
(25) Feyereisen, M.; Fitzgerald, G.; Komornicki, A. *Chem. Phys. Lett.* **1993**, *208*, 359.
(26) Almlöf, J. *Chem. Phys. Lett.* **1991**, *181*, 319.
(27) Jung, Y.; Shao, Y.; Head-Gordon, M. *J. Comput. Chem.* **2007**, *28*, 1953.
(28) Zhang, I. Y.; Xu, X. *Phys. Chem. Chem. Phys.* **2012**, *14*, 12554.
(29) Neese, F.; Schwabe, T.; Grimme, S. *J. Chem. Phys.* **2007**, *126*, 124115.
(30) Lochan, R. C.; Shao, Y.; Head-Gordon, M. *J. Chem. Theory Comput.* **2007**, *3*, 988.
(31) Pople, J. A.; Gill, P. M. W.; Johnson, B. G. *Chem. Phys. Lett.* **1992**, *199*, 557.
(32) Handy, N. C.; Schaefer, H. F. *J. Chem. Phys.* **1984**, *81*, 5031.
(33) Shao, Y.; Fusti-Molnar, L.; Jung, Y.; Kussmann, J.; Ochsenfeld, C.; Brown, S. T.; Gilbert, A. T.; Slipchenko, L. V.; Levchenko, S. V.; O'Neill, D. P.; DiStasio, R. A., Jr; Lochan, R. C.; Wang, T.; Beran, G. J.; Besley, N. A.; Herbert, J. M.; Lin, C. Y.; Van Voorhis, T.; Chien, S. H.; Sodt, A.; Steele, R. P.; Rassolov, V. A.; Maslen, P. E.; Korambath, P. P.; Adamson, R. D.; Austin, B.; Baker, J.; Byrd, E. F. C.; Dachsel, H.; Doerksen, R. J.; Dreuw, A.; Dunietz, B. D.; Dutoi, A. D.; Furlani, T. R.; Gwaltney, S. R.; Heyden, A.; Hirata, S.; Hsu, C.-P.; Kedziora, G.; Khalliulin, R. Z.; Klunzinger, P.; Lee, A. M.; Lee, M. S.; Liang, W.; Lotan, I.; Nair, N.; Peters, B.; Proynov, E. I.; Pieniazek, P. A.; Rhee, Y. M.; Ritchie, J.; Rosta, E.; Sherrill, D. C.; Simmonett, A. C.; Subotnik, J. E.; Woodcock, H. L., III; Zhang, W.; Bell, A. T.; Chakraborty, A. K.; Chipman, D. M.; Keil, F. J.; Warshel, A.; Hehre, W. J.; Schaefer, H. F., III; Kong, J.; Krylov, A. I.; Gill, P. M. W.; Head-Gordon, M. *Phys. Chem. Chem. Phys.* **2006**, *8*, 3172.
(34) Zhao, Y.; Truhlar, D. G. *J. Chem. Phys.* **2006**, *125*, 194101.
(35) Hamprecht, F. A.; Cohen, A. J.; Tozer, D. J.; Handy, N. C. *J. Chem. Phys.* **1998**, *109*, 6264.
(36) Jurecka, P.; Sponer, J.; Cerny, J.; Hobza, P. *Phys. Chem. Chem. Phys.* **2006**, *8*, 1985.
(37) Řezáč, J.; Riley, K. E.; Hobza, P. *J. Chem. Theory Comput.* **2011**, *7*, 2427.
(38) Goerigk, L.; Kruse, H.; Grimme, S. *Chem. Phys. Chem.* **2011**, *12*, 3421.
(39) Hill, J. G.; Peterson, K. A.; Knizia, G.; Werner, H.-J. *J. Chem. Phys.* **2009**, *131*, 194105.
(40) Werner, H.-J.; Knowles, P. J.; Knizia, G.; Manby, F. R.; Schütz, M. *WIREs Comput. Mol. Sci.* **2012**, *2*, 242.